Journal of Applied Physics

RESEARCH ARTICLE | JANUARY 16 2026

Epitaxial growth and physical properties of $Bi_2Ru_2O_7$ thin films on YSZ(111) substrates

Dapeng Cui ; Chengkun Xing; Seunghoon Song ; Dongliang Gong; Shashi Pandey ; Lukas Horák ; Yan Xin ; Haidong Zhou ; Jian Liu

J. Appl. Phys. 139, 035302 (2026)
https://doi.org/10.1063/5.0307901
CHORUS

Journal of Applied Physics ARTICLE pubs.aip.org/aip/jap

Epitaxial growth and physical properties of $Bi_2Ru_2O_7$ thin films on YSZ(111) substrates

Cite as: J. Appl. Phys. **139**, 035302 (2026); doi: 10.1063/5.0307901
Submitted: 19 October 2025 · Accepted: 24 December 2025 ·
Published Online: 16 January 2026

Dapeng Cui,[1,a)] Chengkun Xing,[1] Seunghoon Song,[1] Dongliang Gong,[1] Shashi Pandey,[1] Lukas Horák,[2] Yan Xin,[3] Haidong Zhou,[1] and Jian Liu[1,a)]

AFFILIATIONS

[1]Department of Physics and Astronomy, University of Tennessee, Knoxville, Tennessee 37996, USA
[2]Department of Condensed Matter Physics, Faculty of Mathematics and Physics, Charles University, Prague 12116, Czech Republic
[3]National High Magnetic Field Laboratory, Florida State University, Tallahassee, Florida 32310, USA

[a)]**Authors to whom correspondence should be addressed:** dcui1@utk.edu and jianliu@utk.edu

ABSTRACT

We systematically investigated the growth of $Bi_2Ru_2O_7$ thin films on a Y-stabilized $ZrO_2(111)$ substrate using pulsed laser deposition by mapping the influence of growth temperature and oxygen partial pressure on phase stability, lattice parameters, and cation ratio. The results show that the epitaxial stabilization requires a minimum growth temperature, which is rather insensitive to the pressure. Meanwhile, the Bi:Ru ratio decreases when increasing growth temperature or decreasing pressure. By constructing the temperature–pressure phase diagram, an optimal growth window within the epitaxial phase was established. On the other hand, the electrical resistivity remains at a similar level within the epitaxial phase with only subtle changes to the temperature dependence, indicative of the robustness of the conductivity against composition variation. Our study provides a foundation for future investigations on thin films and heterostructures that utilize $Bi_2Ru_2O_7$.

I. INTRODUCTION

Pyrochlore oxides with the general formula $A_2B_2O_7$ have attracted considerable attention because their interpenetrating A_2O' and B_2O_6 networks (Fig. 1) have great flexibility in the cation combination of the A- and B-sites,[1,2] giving rise to exotic quantum phases, various functional properties, and potential applications.[3–5] Due to the geometrically frustrated lattice, pyrochlore oxides with different A-site cations exhibit diverse electronic and magnetic properties, such as spin ice/liquid,[6–9] spin glass,[10–13] and non-Fermi liquid behavior.[14–17] Replacing the B-site with different transition metals, on the other hand, may tune spin–orbit interaction and electronic correlation, resulting in quantum states such as Weyl semimetals,[18–20] topological Mott insulator,[21,22] and axion insulator.[23,24] In addition to interests in fundamental materials physics, pyrochlore oxides also have demonstrated promising functionalities for applications in catalysis,[25–28] dielectrics,[29–32] and thermoelectrics,[33,34] owing to their tunable carrier density, thermal stability, and high structural symmetry.

In pyrochlore ruthenium oxides $A_2Ru_2O_7$, the A-site cation exerts a decisive role in modulating lattice parameters and Ru–O–Ru bond geometry.[35–37] For instance, insulating or semiconducting behaviors with magnetic orders are typically observed when the A-site is occupied by a rare-earth element (e.g., Pr, Nd, and Y).[38–41] In contrast, a metallic paramagnetic ground state is often stabilized with larger or more covalent A-site ions, such as Bi, Pb, and Tl.[42–44] Although the stereochemically active $6s^2$ long pair may shift the A-site position, such as bismuth-based pyrochlores $Bi_2B_2O_7$ with B = Ti, (Zn/Nb), Sn, and Hf, the Ru–O framework of $Bi_2Ru_2O_7$(BRO) provides sufficient oxygen coordination to satisfy the Bi^{3+} bond-valence requirement, and the lone pair is screened by the conduction electrons, which is similar to the other cases of bismuth-based pyrochlores with heavy metal elements occupying the B-site, e.g., Rh, Ir, and Pt.[45,46] In fact, the combination of electrical conductivity and chemical stability has led to various applications of BRO, such as catalysts/cathode materials,[47–54] bottom electrode material of dielectric layers, and thick-film resistors.[55–58] More recently, Song *et al.*[59] also predicted that BRO could be

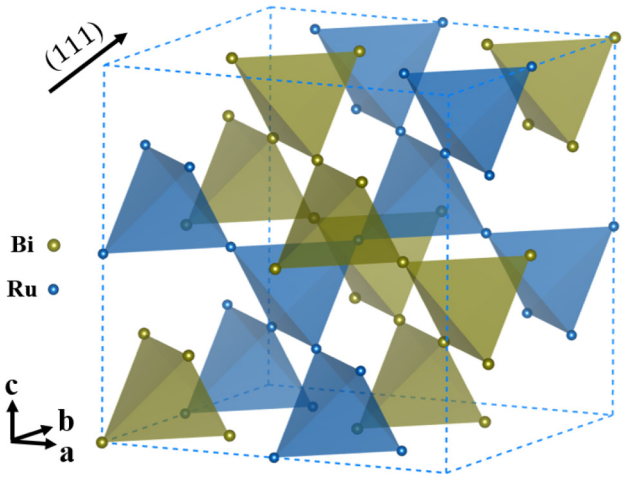

FIG. 1. Schematic illustration of the A-site (Bi) and B-site (Ru) networks of the pyrochlore structure in the $Bi_2Ru_2O_7$ pyrochlore framework. Oxygen atoms are not shown for clarity.

classified into a fragile topological state due to the generalized symmetry eigenvalue criterion, providing motivation to explore its electronic properties. BRO is, thus, an important prototype for investigating itinerant electron behavior in non-magnetic pyrochlores, as well as a candidate for the novel topological state.

Despite these intriguing properties, the thin-film growth of BRO remains poorly understood. To date, few studies on the growth of BRO thin films on pulsed laser deposition (PLD) for epitaxial samples and chemical vapor deposition[60] for polycrystalline samples[55,61] have been reported. The conditions for epitaxial stabilization of BRO have not been systematically investigated. More importantly, potential element loss, particularly due to the volatility of both Bi and Ru, may significantly alter the stoichiometry, for which it is necessary to establish growth control. Reported studies on Bi-based oxides, such as $Bi_2Ir_2O_7$, $BiFeO_3$, and $Bi_2Rh_2O_7$ thin films,[62–64] have revealed that precise control of the temperature and oxygen partial pressure is critical for achieving a stoichiometric cation ratio and stabilizing the epitaxial structure. Similarly, in Ru-base Ruddlesden–Popper system $Sr_{n+1}Ru_nO_{3n+1}$ ($n = 1, 2, \infty$),[65,66] these growth parameters also play a crucial role in stabilizing single-phase films with the desired layering sequence. In this work, we systematically explored the growth of BRO thin films on yttrium-stabilized zirconia (YSZ) substrate using PLD. By mapping the growth phase diagram in terms of temperature and oxygen partial pressure, we identified a narrow window where high-crystallinity and near stoichiometric BRO epitaxial films can be stabilized. The results not only advance the fundamental understanding of BRO thin films but also provide a practical route to utilize volatile-element-based pyrochlore oxides for potential functional devices.

II. EXPERIMENTAL

The BRO thin films were deposited on (111)-oriented YSZ substrates by PLD from a BRO ceramic target made by a solid-state reaction of stoichiometric Bi_2O_3 and RuO_2 powders plus an additional 10% molar ratio of RuO_2. During the deposition, the laser fluence was fixed at 1.3 J/cm^2. We explored the growth conditions by varying the substrate temperature from 450 to 650 °C and oxygen partial pressure from 8×10^{-6} to 1×10^{-3} mbar. Structure analysis by x-ray diffraction (XRD) and the x-ray reflectivity (XRR) were performed using a Panalytical X'Pert MRD diffractometer with an x-ray wavelength of 1.5406 Å using the Cu $K\alpha$ radiation. The cross-sectional transmission electron microscopy (TEM) with electron-dispersive x-ray spectroscopy (EDS) was conducted using a cold field emission probe-aberration-corrected JEOL JEMARM200cF at 200 kV. Temperature-dependent resistivity of the BRO thin films was measured by the four-probe method from 5 to 300 K using a physical property measurement system-Dynacool (PPMS-Dynacool-14T, Quantum Design). Hall measurements were performed in a van der Pauw geometry.

III. RESULTS AND DISCUSSION

We found that the deposition temperature plays the most important role in the epitaxial growth of the pyrochlore phase of BRO (Fig. 1). Figure 2(a) shows the XRR patterns of the BRO thin films deposited under the same oxygen partial pressure at 2×10^{-4} mbar with the same number pulses but at various temperatures. Clear Kiessig fringes were observed for all of them, indicating thin films of similar thicknesses were successfully deposited on the substrates. The thicknesses extracted by fitting to the fringes for the 450, 500, 550, 600, and 650 °C samples are approximately 20.0 (2), 19.8(2), 18.1(3), 19.3(3), and 18.3(3) nm, respectively. The XRD θ–2θ scans, however, showed significant differences as displayed in Fig. 2(b). While the *lll* peaks of the YSZ substrate can be clearly assigned, the *lll* peaks of the pyrochlore BRO phase can only be seen for films deposited at 550 °C or above. Fine scans on these samples around the BRO 222 peak, shown in Fig. 2(c), also revealed pronounced Kiessig fringes, indicating high crystallinity for films deposited at 550 °C or higher. By estimating the film thickness from these fringes,[67] we obtained values consistent with the XRR. In contrast, the presence of fringes in XRR but not in XRD for samples deposited at 450 and 500 °C suggests that these films are amorphous. For samples deposited at 550 °C and above, the BRO peak angle position clearly increases with increasing deposition temperature, illustrating a changing lattice parameter. To obtain the full picture, we performed x-ray reciprocal space mapping (RSM) around the 331 diffraction peak of the substrate, which captures the 662 peak of the BRO pyrochlore phase. As shown in Figs. 2(d)–2(f), Q_z of the film peak increases with increasing temperature, consistent with the θ–2θ scans in Fig. 2(c). Meanwhile, Q_x also increases with increasing temperature toward the position of the substrate peak. Therefore, both the out-of-plane and in-plane lattice parameters increase with increasing growth temperature. This observation shows that the films are relaxed and the deposition temperature significantly affects the unit-cell volume. Another observation is that a very weak peak corresponding to Bi_2O_3 444 appears at 57.7° for the sample deposited at 650 °C. The presence of this minor secondary phase indicates that this temperature is near the upper limit above which impurity phases may appear and the pyrochlore phase may decompose.

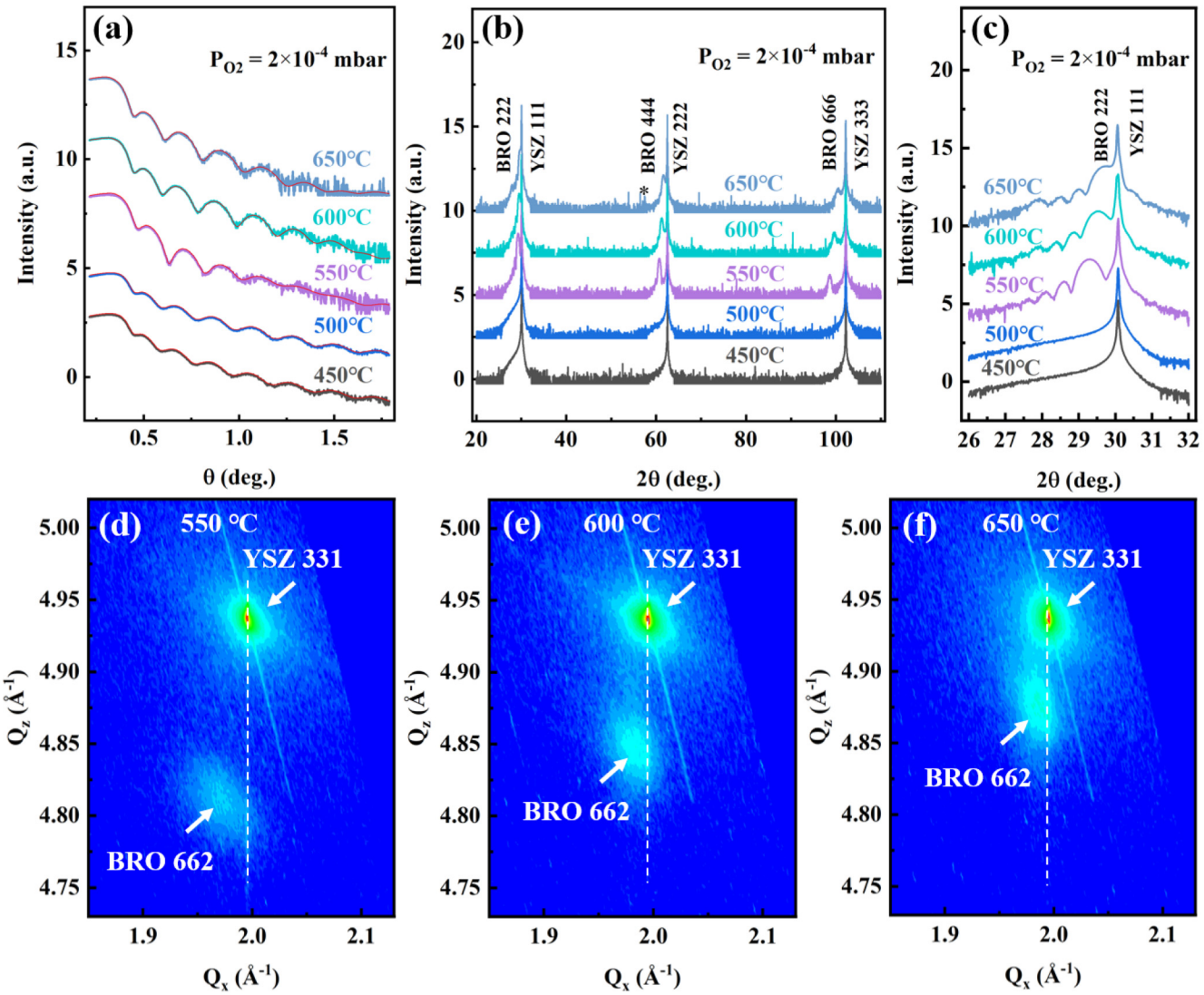

FIG. 2. Structural characterization of BRO thin films grown on YSZ(111) substrates deposited at various temperatures under an oxygen partial pressure of 2×10^{-4} mbar. (a) X-ray reflectivity of BRO films. (b) X-ray diffraction (XRD) θ–2θ scans of BRO films. The asterisk indicates the 444 peak of the Bi_2O_3 secondary phase observed for the 650 °C sample. (c) A fine scan around the 222 peak of the BRO thin films. (d)–(f) Reciprocal space mapping (RSM) of 550, 600, and 650 °C at 2×10^{-4} mbar which around the 331 diffraction peak of the YSZ substrate, showing the BRO 662 diffraction, which demonstrates a partially relaxed strain state. The upper and lower peaks correspond to the YSZ 331 and BRO 662 reflections, respectively. The white dashed line indicates the fully strained condition for the films where supposed to be located.

Tuning the growth temperature under other oxygen partial pressure at 1×10^{-3}, 5×10^{-5}, and 8×10^{-6} mbar yields similar results [Fig. S1 in the supplementary material], which confirms the dominant role of growth temperature in stabilizing the pyrochlore BRO phase.

Based on the results above, the epitaxial growth of BRO thin films with well-defined crystallographic orientation can be achieved above a critical temperature around 550 °C and within a rather broad pressure range that spans at least three orders of magnitude. Indeed, as illustrated in the θ–2θ scans on films grown at 600 °C and different pressures as the examples [Figs. 3(a) and 3(b)], all films exhibit clear diffraction peaks and Kiessig fringes, confirming high crystalline quality within the entire investigated pressure range. The oxygen partial pressure does not affect the phase stabilization in any significant way other than very small shifts of the peak position. This is confirmed by the RSMs shown in Figs. 3(f)–3(i), where the film peak hardly moves along either Q_z or Q_x with pressure. Figures 3(c)–3(e) summarize the extracted

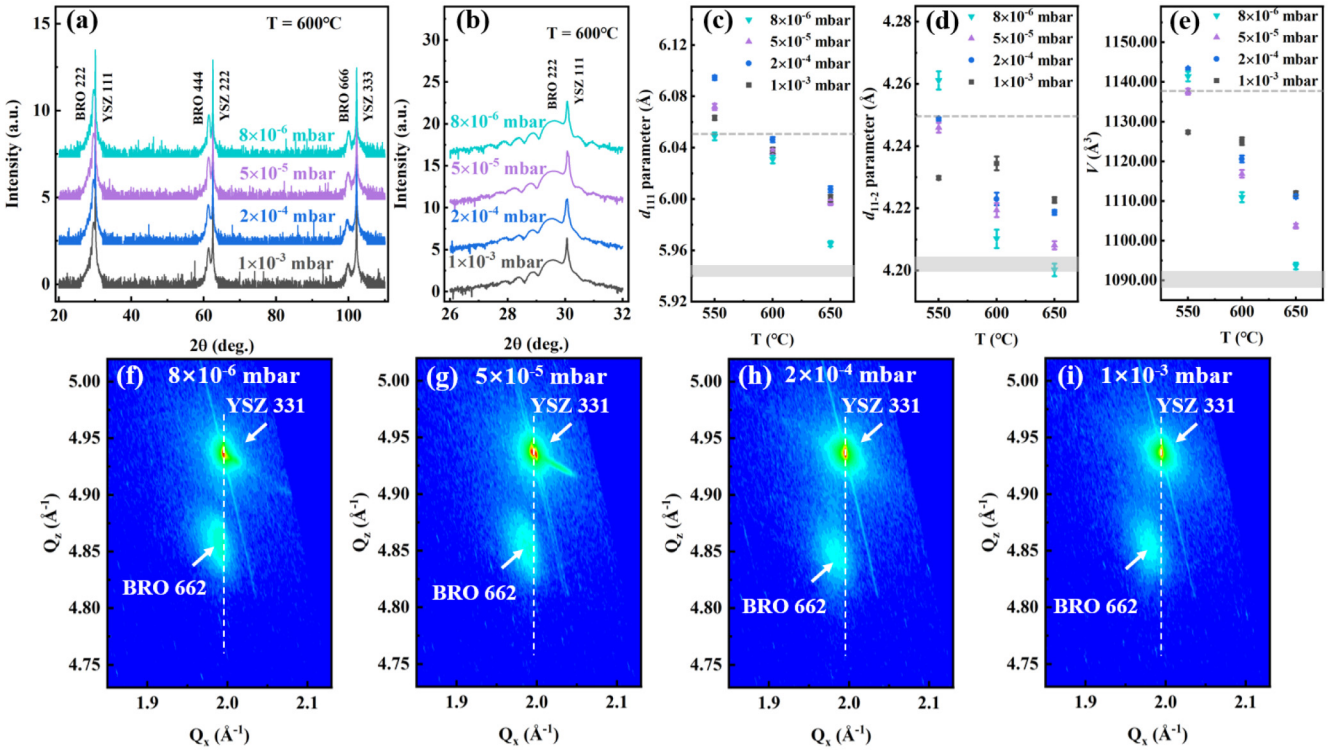

FIG. 3. (a) Structural characterization of BRO thin films grown on YSZ(111) substrates deposited at various oxygen partial pressures under the temperature of 650 °C. (b) A fine scan around the 222 peak of the BRO thin films in figure (a). (c)–(e) Calculated lattice parameter d_{111}, $d_{11\bar{2}}$, and lattice volume V of BRO films as a function of deposited temperature under different oxygen partial pressure. Gray shaded bands and gray dashed lines are bulk and film reference values.[44,60,68,69] (f)–(i) Reciprocal space mapping (RSM) of the 8×10^{-6}, 5×10^{-5}, 2×10^{-4}, and 1×10^{-3} mbar at 600 °C, which is around the 331 diffraction peak of the YSZ substrate, showing the BRO 662 diffraction, which demonstrates a partially relaxed strain state. The upper and lower peaks correspond to the YSZ 331 and BRO 662 reflections, respectively. The white dashed line indicates the fully strained condition for the films where supposed to be located.

lattice parameters and unit cell volume of all investigated combinations of growth temperature and pressure where the epitaxial phase is stabilized. We note that for BRO, the films are relaxed from the substrate possibly due to slight cation off stoichiometry, justifying the film lattice parameters' comparison with those of the bulk and the film.[44,60,68,69] One can see that the lattice parameter change overall follows the volume change, and the pressure-induced change is much smaller than the difference when changing the growth temperature. While this result demonstrates a systematic control of the epitaxial growth, XRD alone is clearly insufficient to resolve the evolution underneath the lattice parameter variation within the growth phase space.

To further distinguish the differences within the growth phase space, we measured high-resolution TEM and EDS on representative BRO thin film samples. First, the sample grown at 450 °C under 1×10^{-3} mbar exhibited an amorphous microstructure as shown in Fig. 4(a). This is consistent with the XRD result and is expected for all samples grown at 450 and 500 °C below the critical temperature of epitaxial stabilization regardless of the oxygen partial pressure. More importantly, this sample has a Bi-rich composition (Bi : Ru = 55.6% : 44.4%). Since the Ru ionic radius is smaller than Bi and the unit cell volume is mainly controlled by the growth temperature, its temperature-driven change could be related to the Bi:Ru ratio. To test this hypothesis, we investigated a sample grown at 650 °C. As shown in Fig. 4(b), this sample exhibits a clear epitaxial structure, which is also consistent with XRD. It has a Bi:Ru ratio of 46.0%:54.0%, which is not only much lower but also Ru-rich. These results suggest that growth at lower temperatures close to the critical temperature of phase stabilization may bring the Bi:Ru ratio closer to 1:1 for an epitaxial film. To explore such an optimization, we tuned the growth temperature to 575 °C while maintaining the oxygen partial pressure the same as the 650 °C sample. The obtained sample as shown in Fig. 4(c) has a Bi:Ru ratio equal to 51.2%:48.8%, which is very close to the ideal 1:1 stoichiometry within the error of EDS. Notably, this sample also maintains good crystalline quality and a sharp interface with the substrate. The decrease in the Bi:Ru ratio with increasing growth temperature is in fact consistent with the contraction of the lattice parameter and the unit-cell volume. These results suggest the ideal growth temperature is around 575–600 °C. Finally, to evaluate the impact of the pressure, we measured a sample deposited at 600 °C but under 8×10^{-6} mbar, which is the lower end of the investigated

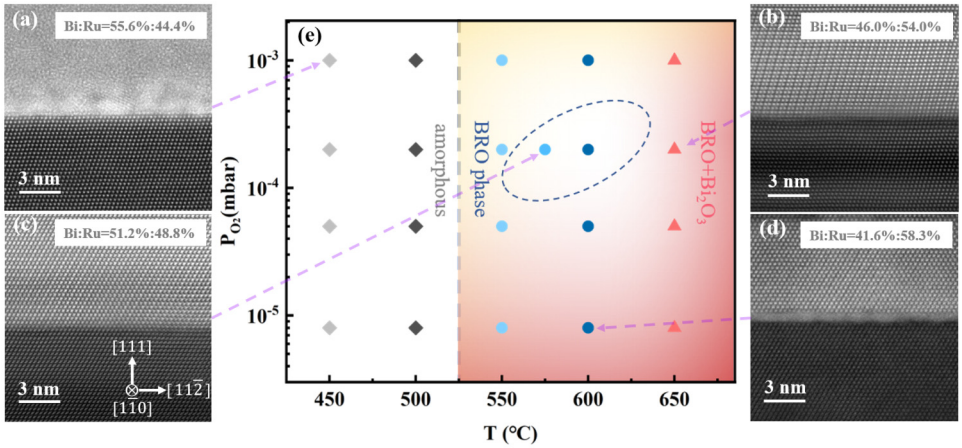

FIG. 4. Cross section HAADF-STEM images of the BRO thin films growth on the YSZ(111) substrate. (a) Oxygen partial pressure under 1×10^{-3} mbar at 450 °C. (b) Oxygen partial pressure under 2×10^{-4} mbar at 650 °C. (c) Oxygen partial pressure under 2×10^{-4} mbar at 575 °C. (d) Oxygen partial pressure under 8×10^{-6} mbar at 600 °C. Crystal axes are shown in Fig. 4(c). The corresponding elemental compositions were extracted via energy-dispersive x-ray spectroscopy (EDS) and are annotated in each figure. (e) Growth phase diagram of the Bi-Ru-O system as functions of substrate temperature T and oxygen pressure P_{O_2}, classified into two regions. Triangles denote the BRO phase with a minor Bi_2O_3 secondary phase, circles denote the pure BRO phase, and diamonds denote the amorphous phase. The background color illustrates the general trend of the cation ratio within the epitaxial region.

range. As shown in Fig. 4(d), despite a less coherent interface with the YSZ substrate, it still has an epitaxial structure, consistent with XRD. Meanwhile, the Bi:Ru ratio (41.6%:58.4%) drops significantly back down, indicating that lowering oxygen pressure decreases the Bi:Ru ratio as well similar to increasing temperature. These observations indicate that Ru deficiency is the main stoichiometric challenge even with 10% extra Ru in the target as opposed to extra Bi. Without that, one may need to increase the temperature further, which, however, may reach the regime where Bi-rich secondary phases start to appear as indicated by XRD.

Figure 4(e) summarizes the growth phase diagram of BRO thin films constructed from the combined results of structural and compositional analysis. The deposition behavior of BRO thin films can be broadly categorized into two regimes. At temperatures around 500 °C and below, the films tend to be amorphous. This could be attributed to insufficient surface diffusion and inadequate thermal energy for crystallization, resulting in poor nucleation and growth kinetics.[70] Above this temperature, the films tend to be epitaxial and single-phase until a minor secondary appears at 650 °C. This critical temperature of epitaxial stabilization is in contrast to other ruthenates, for which lower deposition temperatures are more favorable because of the suppression of the volatility of ruthenium during the thin film growth.[65,66] The fact that the Bi/Ru ratio decreases with increasing temperature indicates that the bismuth volatility is a more serious issue than the ruthenium volatility for the growth of BRO at elevated temperatures. A similar evolution has also been reported for Bi–Rh–O thin films,[71] suggesting a common need to balance the cation volatility in Bi-based oxides. Indeed, similar temperature and oxygen pressure dependence has also been reported in other Bi-base multiferroic system, such as $BiFeO_3$ and Bi_2FeCrO_6.[72,73] In these systems, the Bi concentration was found to decrease with increasing temperature at a constant

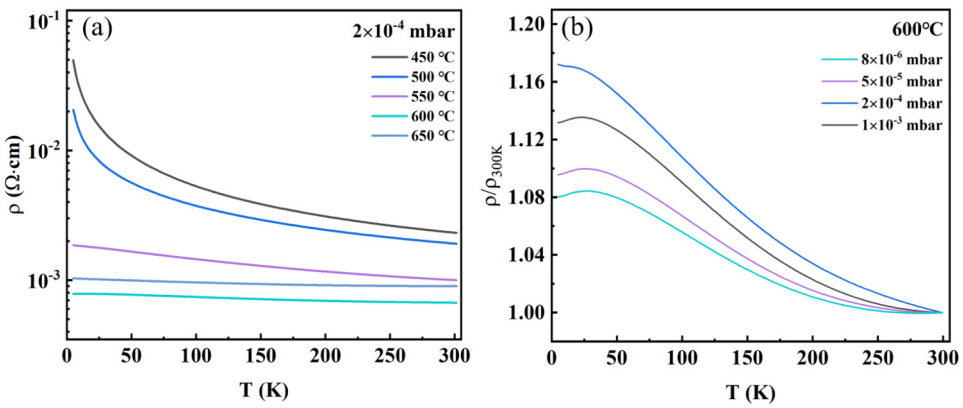

FIG. 5. (a) Temperature-dependent resistivity ρ(T) curves of the BRO thin films grown at 2×10^{-4} mbar under different deposition temperatures. (b) Temperature-dependent normalized resistivity ρ(T) curves of the BRO thin films grown at 600 °C under various oxygen pressures.

oxygen pressure and increase with rising oxygen pressure at the same temperature. The Bi/Ru evolution observed in our BRO thin films is reminiscent of this behavior. Furthermore, in the case of $BiFeO_3$,[74] the decrease in the Bi content with reduced oxygen pressure was consistent with the decrease in the unit-cell volume and the crystallinity of the films, similar to our observation in the Bi/Ru system shown in Fig. 3. Notably, high-quality epitaxial films in $BiFeO_3$ and Bi_2FeCrO_6 systems have also been achieved under optimized conditions involving a relatively narrow growth window at intermediate oxygen pressure and temperature, similar to the ideal growth window identified in our BRO growth diagram. Nonetheless, this growth diagram provides a comprehensive guide for controlling the epitaxial stabilization and the Bi/Ru stoichiometry in BRO thin films.

Having established the growth phase diagram, we investigated the temperature-dependent resistivity ρ(T). A representative dataset of growth temperature-dependence is shown in Fig. 5(a). One can see a clear distinction between the amorphous and epitaxial films when increasing the growth temperature from 450 to 650 °C. Specifically, the amorphous films show an insulating behavior as the resistivity increases exponentially by one order of magnitude from 300 to 5 K. The epitaxial films, on the other hand, are much more conductive. The resistivity is around 10^{-4}–10^{-3} Ω cm and varies little with temperature. These behaviors of the epitaxial films are overall consistent with the literature,[44,55,60,75,76] which reported a variety of temperature-dependent behaviors even for bulk samples where the resistivity may increase and/or decrease slightly upon cooling but always within the same range. For instance, the resistivity of our film grown at 600 °C increases very slowly with decreasing temperature, and it appears to approach some maximal level near 5 K, which is consistent with the reported epitaxial film samples on YSZ.[60] Samples grown at different pressures also display very similar behavior as shown in Fig. 5(b). In general, our results show that, within the epitaxial phase of the growth phase diagram [Fig. 4(e)], the films all show a similar level of resistivity and relatively weak temperature dependence despite the significant variations in the cation ratio. This observation highlights the robustness of the conductivity of the BRO epitaxial films. Hall measurements on the samples grown at 600 °C under 2×10^{-4} and 8×10^{-6} mbar show that they have similar carrier density of the electron-type and similar mobility as shown in Fig. S3 in the supplementary material. The lower pressure one has slightly higher carrier density and mobility, which could be related to the different Bi:Ru ratios. The temperature dependence of the carrier density and mobility are similar to the reported results on thick BRO films.[60]

IV. CONCLUSION

In summary, we have demonstrated the epitaxial growth of BRO thin films on YSZ(111) substrates via PLD. By systematically tuning the growth temperature and oxygen partial pressure, we showed that a similar critical temperature must be reached to stabilize the epitaxial growth regardless of the pressure. The films also exhibit a systematic variation of cation ratio controllable by the growth temperature and oxygen partial pressure. Our results identify an optimal growth condition near 575–600 °C and 2×10^{-4} mbar. Transport measurement, however, shows that the electrical resistivity of the BRO film is rather insensitive to the growth condition within the investigated parameter range as long as the film is epitaxial. This study highlights the pivotal role of growth parameters in stabilizing Bi-based pyrochlore and functional oxide thin films. Furthermore, integrating BRO films into heterostructures and device architectures could open pathways for novel oxide electronics and energy-related applications.

SUPPLEMENTARY MATERIAL

SEE the Supplementary Material for additional datasets. Figure S1 in the supplementary material shows x-ray diffraction θ–2θ scans and x-ray reflectivity of BRO films grown at 450–650 °C under 1×10^{-3} mbar, 5×10^{-5} mbar, and 8×10^{-6} mbar. Figure S2 in the supplementary material presents high-resolution θ–2θ scans around the YSZ 222 and BRO 444 reflections at 650 °C under 1×10^{-3}, 2×10^{-4}, 5×10^{-5}, and 8×10^{-6} mbar with Bi_2O_3 highlighted by asterisks. Figure S3 in the supplementary material includes a linear negative Hall signal at 40 K for two films grown at 600 °C under 2×10^{-4} and 8×10^{-6} mbar, the extracted single-band carrier density and mobility from 10 to 80 K.

ACKNOWLEDGMENTS

This research was supported by the U.S. Department of Energy under Grant No. DE-SC0020254. Part of the work was done in the National High Magnetic Field Laboratory, which is supported by the National Science Foundation (NSF) Cooperative Agreement Nos. DMR-2128556 and DMR-1644779, and the State of Florida. We gratefully thank Ms. Charlotte Buchanan and Professor Dustin Gilbert for the assistance on Hall measurements.

AUTHOR DECLARATIONS

Conflict of Interest

The authors have no conflicts to disclose.

Author Contributions

Dapeng Cui: Data curation (equal); Formal analysis (equal); Investigation (equal); Methodology (equal); Project administration (equal); Validation (equal); Visualization (equal); Writing – original draft (equal); Writing – review & editing (equal). **Chengkun Xing:** Conceptualization (supporting); Data curation (supporting); Investigation (supporting); Methodology (supporting); Validation (supporting); Visualization (supporting); Writing – original draft (supporting); Writing – review & editing (supporting). **Seunghoon Song:** Investigation (supporting); Resources (supporting); Writing – original draft (supporting). **Dongliang Gong:** Formal analysis (supporting); Investigation (supporting); Methodology (supporting); Writing – original draft (supporting). **Shashi Pandey:** Investigation (supporting); Methodology (supporting); Writing – review & editing (supporting). **Lukas Horák:** Formal analysis (equal); Investigation (equal); Validation (equal); Writing – review & editing (supporting). **Yan Xin:** Investigation (equal); Validation (supporting); Visualization (supporting); Writing – review & editing (supporting).

Haidong Zhou: Conceptualization (lead); Funding acquisition (equal); Project administration (equal); Supervision (equal); Writing – original draft (supporting); Writing – review & editing (supporting). **Jian Liu:** Conceptualization (equal); Formal analysis (equal); Funding acquisition (equal); Methodology (equal); Project administration (equal); Supervision (equal); Validation (equal); Visualization (equal); Writing – original draft (equal); Writing – review & editing (equal).

DATA AVAILABILITY

The data that support the findings of this study are available from the corresponding authors upon reasonable request.

REFERENCES

[1]M. V. Talanov and V. M. Talanov, Chem. Mater. **33**, 2706 (2021).
[2]M. A. Subramanian, G. Aravamudan, and G. V. Subba Rao, Prog. Solid State Chem. **15**, 55 (1983).
[3]J. S. Gardner, M. J. P. Gingras, and J. E. Greedan, Rev. Mod. Phys. **82**, 53 (2010).
[4]W. Witczak-Krempa, G. Chen, Y. B. Kim, and L. Balents, Annu. Rev. Condens. Matter Phys. **5**, 57 (2014).
[5]J. Chakhalian, X. Liu, and G. A. Fiete, APL Mater. **8**, 050904 (2020).
[6]Y. Machida, S. Nakatsuji, S. Onoda, T. Tayama, and T. Sakakibara, Nature **463**, 210 (2010).
[7]S. Legl, C. Krey, S. R. Dunsiger, H. A. Dabkowska, J. A. Rodriguez, G. M. Luke, and C. Pfleiderer, Phys. Rev. Lett. **109**, 047201 (2012).
[8]M. J. P. Gingras and P. A. McClarty, Rep. Prog. Phys. **77**, 056501 (2014).
[9]D. P. Leusink, F. Coneri, M. Hoek, S. Turner, H. Idrissi, G. Van Tendeloo, and H. Hilgenkamp, APL Mater. **2**, 032101 (2014).
[10]D. K. Singh and Y. S. Lee, Phys. Rev. Lett. **109**, 247201 (2012).
[11]Y. M. Jana, O. Sakai, R. Higashinaka, H. Fukazawa, Y. Maeno, P. Dasgupta, and D. Ghosh, Phys. Rev. B **68**, 174413 (2003).
[12]H. Silverstein, K. Fritsch, F. Flicker, A. Hallas, J. S. Gardner, Y. Qiu, G. Ehlers, A. Savici, Z. Yamani, K. Ross *et al.*, Phys. Rev. B **89**, 054433 (2014).
[13]P. M. Thygesen, J. A. Paddison, R. Zhang, K. A. Beyer, K. W. Chapman, H. Y. Playford, M. G. Tucker, D. A. Keen, M. A. Hayward, and A. L. Goodwin, Phys. Rev. Lett. **118**, 067201 (2017).
[14]T. F. Qi, O. B. Korneta, X. Wan, L. E. DeLong, P. Schlottmann, and G. Cao, J. Phys.: Condens. Matter. **24**, 345601 (2012).
[15]T. Ohtsuki, Z. Tian, A. Endo, M. Halim, S. Katsumoto, Y. Kohama, K. Kindo, M. Lippmaa, and S. Nakatsuji, Proc. Natl. Acad. Sci. U.S.A. **116**, 8803 (2019).
[16]J. M. Ni, Y. Y. Huang, E. J. Cheng, Y. J. Yu, B. L. Pan, Q. Li, L. M. Xu, Z. M. Tian, and S. Y. Li, Nat. Commun. **12**, 307 (2021).
[17]H. Shinaoka, S. Hoshino, M. Troyer, and P. Werner, Phys. Rev. Lett. **115**, 156401 (2015).
[18]B.-J. Yang and N. Nagaosa, Phys. Rev. Lett. **112**, 246402 (2014).
[19]X. Liu, S. Fang, Y. Fu, W. Ge, M. Kareev, J.-W. Kim, Y. Choi, E. Karapetrova, Q. Zhang, L. Gu *et al.*, Phys. Rev. Lett. **127**, 277204 (2021).
[20]T.-C. Wu, Y. Chang, A.-K. Wu, M. Terilli, F. Wen, M. Kareev, E. S. Choi, D. Graf, Q. Zhang, L. Gu *et al.*, Sci. Adv. **11**, eadr6202 (2025).
[21]H.-M. Guo and M. Franz, Phys. Rev. Lett. **103**, 206805 (2009).
[22]B.-J. Yang and Y. B. Kim, Phys. Rev. B **82**, 085111 (2010).
[23]X. Wan, A. M. Turner, A. Vishwanath, and S. Y. Savrasov, Phys. Rev. B **83**, 205101 (2011).
[24]N. Varnava and D. Vanderbilt, Phys. Rev. B **98**, 245117 (2018).
[25]J. Park, M. Risch, G. Nam, M. Park, T. J. Shin, S. Park, M. G. Kim, Y. Shao-Horn, and J. Cho, Energy Environ. Sci. **10**, 129 (2017).
[26]P. Gayen, S. Saha, and V. Ramani, ACS Appl. Energy Mater. **3**, 3978 (2020).
[27]J. Kim, P.-C. Shih, Y. Qin, Z. Al-Bardan, C.-J. Sun, and H. Yang, Angew. Chem. Int. Ed. **57**, 13877 (2018).
[28]K. Sardar, E. Petrucco, C. I. Hiley, J. D. B. Sharman, P. P. Wells, A. E. Russell, R. J. Kashtiban, J. Sloan, and R. I. Walton, Angew. Chem. **126**, 11140 (2014).
[29]I. Levin, T. G. Amos, J. C. Nino, T. A. Vanderah, C. A. Randall, and M. T. Lanagan, J. Solid State Chem. **168**, 69 (2002).
[30]M. T. Weller, R. W. Hughes, J. Rooke, C. S. Knee, and J. Reading, Dalton Trans. **19**, 3032 (2024).
[31]A. L. Hector and S. B. Wiggin, J. Solid State Chem. **177**, 139 (2004).
[32]S. J. Henderson, O. Shebanova, A. L. Hector, P. F. McMillan, and M. T. Weller, Chem. Mater. **19**, 1712 (2007).
[33]Y. Zhou, I. Matsubara, R. Funahashi, and S. Sodeoka, Mater. Lett. **51**, 347 (2001).
[34]M. Yasukawa, S. Kuniyoshi, and T. Kono, Solid State Commun. **126**, 213 (2003).
[35]B. J. Kennedy and T. Vogt, J. Solid State Chem. **126**, 261 (1996).
[36]K.-S. Lee, D.-K. Seo, and M.-H. Whangbo, J. Solid State Chem. **131**, 405 (1997).
[37]F. Ishii and T. Oguchi, J. Phys. Soc. Jpn. **69**, 526 (2000).
[38]M. Tachibana, H. Kawaji, and T. Atake, Phys. Rev. B **71**, 060402 (2005).
[39]J. S. Lee, S. J. Moon, T. W. Noh, T. Takeda, R. Kanno, S. Yoshii, and M. Sato, Phys. Rev. B **72**, 035124 (2005).
[40]M. W. Gaultois, P. T. Barton, C. S. Birkel, L. M. Misch, E. E. Rodriguez, G. D. Stucky, and R. Seshadri, J. Phys.: Condens. Matter **25**, 186004 (2013).
[41]G. Laurita, D. Puggioni, D. Hickox-Young, J. M. Rondinelli, M. W. Gaultois, K. Page, L. K. Lamontagne, and R. Seshadri, Phys. Rev. Mater. **3**, 095003 (2019).
[42]T. Takeda, M. Nagata, H. Kobayashi, R. Kanno, Y. Kawamoto, M. Takano, T. Kamiyama, F. Izumi, and A. W. Sleight, J. Solid State Chem. **140**, 182 (1998).
[43]J. Okamoto, T. Mizokawa, A. Fujimori, T. Takeda, R. Kanno, F. Ishii, and T. Oguchi, Phys. Rev. B **69**, 035115 (2004).
[44]M. Tachibana, Y. Kohama, T. Shimoyama, A. Harada, T. Taniyama, M. Itoh, H. Kawaji, and T. Atake, Phys. Rev. B **73**, 193107 (2006).
[45]B. B. Hinojosa, J. C. Nino, and A. Asthagiri, Phys. Rev. B **77**, 104123 (2008).
[46]D. P. Shoemaker, R. Seshadri, M. Tachibana, and A. L. Hector, Phys. Rev. B—Condens. Matter Mater. Phys. **84**, 064117 (2011).
[47]J. Park, H. Jang, S. Y. Lee, J. S. Jeon, and M. G. Kim, J. Mater. Chem. A **10**, 561 (2022).
[48]S. H. Oh, R. Black, E. Pomerantseva, J.-H. Lee, and L. F. Nazar, Nat. Chem. **4**, 1004 (2012).
[49]A. Jaiswal and E. D. Wachsman, Ionics **15**, 1 (2009).
[50]V. Esposito, B. H. Luong, E. Di Bartolomeo, E. D. Wachsman, and E. Traversa, J. Electrochem. Soc. **153**, A2232 (2006).
[51]T. Takeda, R. Kanno, K. Tsubosaka, and Y. Takeda, Electrochemistry **70**, 969 (2002).
[52]A. Widelöv, N. M. Markovic, and P. N. Ross, J. Electrochem. Soc. **143**, 3504 (1996).
[53]N. M. Marković and P. N. Ross, J. Electrochem. Soc. **141**, 2590 (1994).
[54]G. Gökağaç and B. J. Kennedy, J. Electroanal. Chem. **368**, 235 (1994).
[55]M. Nakajima, R. Ikariyama, P. Sankara Rama Krishnan, T. Yamada, and H. Funakubo, Appl. Phys. Lett. **104**, 022908 (2014).
[56]G. E. Pike and C. H. Seager, J. Appl. Phys. **48**, 5152 (1977).
[57]P. F. Carcia, A. Ferretti, and A. Suna, J. Appl. Phys. **53**, 5282 (1982).
[58]Z. Stanimirović and I. Stanimirović, IEEE Trans. Electron Devices **67**, 600 (2019).
[59]Z.-D. Song, L. Elcoro, Y.-F. Xu, N. Regnault, and B. A. Bernevig, Phys. Rev. X **10**, 031001 (2020).
[60]M. O'Sullivan, J. Alaria, M. S. Dyer, J. B. Claridge, M. W. Gaultois, and M. J. Rosseinsky, APL Mater. **11**, 050702 (2023).
[61]H. Chiba, R. Ikariyama, S. Yasui, and H. Funakubo, Thin Solid Films **669**, 471 (2019).
[62]W. C. Yang, Y. T. Xie, W. K. Zhu, K. Park, A. P. Chen, Y. Losovyj, Z. Li, H. M. Liu, M. Starr, J. A. Acosta *et al.*, Sci. Rep. **7**, 7740 (2017).
[63]W. C. Yang, Y. T. Xie, X. Sun, X. H. Zhang, K. Park, S. C. Xue, Y. L. Li, C. G. Tao, Q. X. Jia, Y. Losovyj *et al.*, Phys. Rev. Mater. **2**, 114206 (2018).
[64]M. Ohno, T. Fujita, and M. Kawasaki, Appl. Phys. Lett. **122**, 251601 (2023).

[65]D. G. Schlom, Y. Jia, L. Zou, J. Hanei, S. Briczinski, M. Zurbuchen, C. W. Leitz, S. Madhavan, S. Wozniak, Y. Liu *et al.*, in *Superconducting and Related Oxides: Physics and Nanoengineering III* (SPIE, 1998), Vol. 3481, pp. 226–240.
[66]T. Ohnishi and K. Takada, Appl. Phys. Express **4**, 025501 (2011).
[67]D. Cui, M. Gu, C. Li, H. Duan, W. Yan, P. Wang, A. Li, and D. Wu, J. Phys.: Condens. Matter **31**, 245002 (2019).
[68]R. J. Bouchard and J. L. Gillson, Mater. Res. Bull. **6**, 669 (1971).
[69]B. Řehák, K. Horčic, M. Frumar, and L. Koudelka, J. Cryst. Growth **68**, 647 (1984).
[70]R. Eason, *Pulsed Laser Deposition of Thin Films: Applications-Led Growth of Functional Materials* (John Wiley & Sons, 2006).
[71]M. Uchida, K. Ohba, Y. Ohuchi, Y. Kozuka, and M. Kawasaki, Chem. Mater. **28**, 1165 (2016).
[72]H. Béa, M. Bibes, A. Barthélémy, K. Bouzehouane, E. Jacquet, A. Khodan, J.-P. Contour, S. Fusil, F. Wyczisk, A. Forget *et al.*, Appl. Phys. Lett. **87**, 072508 (2005).
[73]R. Nechache, C. Harnagea, L.-P. Carignan, O. Gautreau, L. Pintilie, M. P. Singh, D. Ménard, P. Fournier, M. Alexe, and A. Pignolet, J. Appl. Phys. **105**, 061621 (2009).
[74]L. You, N. T. Chua, K. Yao, L. Chen, and J. Wang, Phys. Rev. B **80**, 024105 (2009).
[75]M. K. Haas, R. J. Cava, M. Avdeev, and J. D. Jorgensen, Phys. Rev. B **66**, 094429 (2002).
[76]X. Gai, J. Qu, N. Zhang, C. You, F. Zhang, T. Lv, Q. Tao, P. Zhu, Y. Li, and X. Wang, J. Phys. Chem. C **128**, 7306 (2024).